Preprints of the 19th World Congress
The International Federation of Automatic Control
Cape Town, South Africa. August 24-29, 2014

Nonlinear Characteristic Model–Based SMC and Its Application to Flexible Satellites ⋆

L. Chen * **Y. Yan** * **C.Y. Sun** *

* *School of Automation, Southeast University, Nanjing, 210096, China (e-mail: parisalexander@163.com, yy_spring@163.com, cysun@seu.edu.cn).*

Abstract: This study investigates the sliding mode control (SMC) method based on the nonlinear characteristic model and its application to flexible satellites. A novel nonlinear dynamic sliding mode surface is designed depending on the nonlinear characteristic model. The expected advantage of the proposed SMC compared to the traditional SMC is to improve performances and robustness. The proposed results apply to a class of nonlinear systems and rely on the parameter estimation of the characteristic model. The theory is illustrated on the rapid maneuver and fast stability problem of the sun synchronous orbit satellite.

Keywords: Sliding mode control, Characteristic model, Flexible satellite, Rapid maneuver.

1. INTRODUCTION

In recent years, control problems for nonlinear systems have attracted a great deal of interest, which is motivated by their different types of applications (see, e.g., Sun et al. [2013]), such as hypersonic vehicles, flexible satellites, and power systems. To improve the performances of the close–loop system, many nonlinear control methods, such as adaptive control in Chen et al. [2009], optimal control in Luo et al. [2005], and output feedback control in Wong et al. [2001] have been employed. It is well known that SMC is an efficient method to deal with nonlinear systems with external disturbances and parametric uncertainties (see, e.g., Yu et al. [2012]). Usually, a linear sliding mode surface is employed to design a controller for nonlinear systems (see Xia et al. [2011]). In order to enhance the performance of the SMC system, a solution is to employ nonlinear sliding mode manifolds. For example, the terminal SMC has advantages of fast convergence and better disturbance rejection performance (see, e.g., Zhang et al. [2012] for a detailed discussion).

For some controlled plant, it is not easy or possible to depict their dynamics and environment with mathematical models, and for some others, even if they can be represented by accurate mathematical models, the order of the models is usually very high and the structure is very complicated. Therefore, the theory of characteristic modeling, as a kind of data–based model–free approach for control system design, was proposed in Wu et al. [2001]. It requires the analysis of the dynamic and control performance of the system instead of an accurate plant dynamic analysis. Based on this methodology, a golden section adaptive control method, which aims at designing an engineering–oriented adaptive controller by using only a few parameters, has been successfully used in various industries (see, e.g., Meng et al. [2009]).

The satellite attitude control problem includes attitude stabilization and attitude tracking (see Wen et al. [1991]), and the latter has important applications in particular. In terms of satellite attitude tracking tasks, large angle or fast angular rate will generally be considered in the rotation process. Therefore, the cross coupling terms in the dynamic and kinematic equations become significant and cannot be neglected, which make the system turn out to be highly nonlinear (see, e.g., Zhang et al. [2013]). System uncertainties and external disturbances are two further challenges to be addressed in the design of attitude controllers. Furthermore, the orbiting attitude slewing operation introduces vibration in the flexible appendages, which may degrade the attitude pointing accuracy. Since an attitude control law based on linearisation and nonlinear inversion was presented in Singh [1988], many investigations using various controllers to design spacecraft attitude control laws have been available (see, e.g., Hu et al. [2012], Peaucelle et al. [2011], and Zanchettin et al. [2011]).

In this paper, by introducing a nonlinear sliding mode surface based on characteristic modeling, the SMC method is proposed for the tracking control of a class of nonlinear systems. Firstly, according to the characteristic modeling method, the characteristic model of a class of nonlinear systems is established and the parameters of the model are obtained by the recursive least–square method. Secondly, a characteristic model–based nonlinear sliding mode is designed and Lyapunov stability law is applied to tackle the problem how the states can reach the sliding surface. Furthmore, an application to a nonlinear system is verified by simulation results, which also facilitates the analysis of the nonlinear sliding surface. Finally, the proposed

⋆ This work was supported by National Natural Science Foundation of China (Project 61125306, 91016004) and Ph.D. Programs Foundation of Ministry of Education of China(Project 20110092110020, 20120092110026)

controller is used for the attitude control problem of flexible satellites.

2. PRELIMINARIES AND PROBLEM FORMULATION

2.1 Characteristic Modeling

Consider the nonlinear system

$$\dot{x}(t) = f(x, \dot{x}, \cdots, x^{(n)}, u, \dot{u}, \cdots, u^{(m)}), \tag{1}$$

where x and u denote the state and input of the system, respectively. Choosing

$$\begin{aligned} x = x_1, \dot{x} = x_2, \cdots, x^{(n)} = x_n + 1 \\ u = u_1, \dot{u} = u_2, \cdots, u^{(m)} = u_m + 1 \end{aligned} \tag{2}$$

then (1) can be written as

$$\dot{x}_1(t) = f(x_1, \cdots, x_n + 1, u_1, \cdots, u_m + 1). \tag{3}$$

Assume that the characters of the nonlinear system (3) are as follows (see Wu et al. [2001]):

(a) There are only a single input and a single output.
(b) The power of $u(t)$ is 1.
(c) If $x_i = 0$ and $u_i = 0$, we have $f(\cdot) = 0$.
(d) $f(\cdot)$ is continuously differentiable to all variables, and partial derivative values are bounded.
(e) $\mid f(x(t + \triangle t), u(t + \triangle t)) \mid - \mid f(x(t), u(t)) \mid < M \triangle t$, where the constant $M > 0$ and $\triangle t$ is sampling time.
(f) The states and control value are bounded.

Based on (3), the following lemmas will be used in the derivation of the main results.

Lemma 1. (see Wu et al. [2001]) For any nonlinear system that can be described as (1), if assumptions (a)–(d) are satisfied and sampling time $\triangle t$ satisfies certain conditions, its characteristic model can be expressed with the following 2–order difference equation,

$$x(k+1) = f_1(k)x(k) + f_2(k)x(k-1) + g_0(k)u(k) + g_1(k)u(k-1). \tag{4}$$

If the system is stable and assumptions (e)–(f) are satisfied, then

- $f_1(k)$, $f_2(k)$, $g_0(k)$, and $g_1(k)$ are parameters of the characteristic model and are slowly time varying.
- The ranges of these coefficients can be determined beforehand.
- In dynamic process, under the same input, selecting suitable sampling period $\triangle t$ can make sure that the output error between the characteristic model and the controlled plant keeps within a permitted limit.
- In steady state, both outputs are equal.

For the minimum–phase system, in general the characteristic model is chosen as follows:

$$x(k+1) = f_1(k)x(k) + f_2(k)x(k-1) + g_0(k)u(k). \tag{5}$$

Lemma 2. (see Wu et al. [2001]) For any nonlinear system that can be described as (1), if assumptions (1)–(4) are satisfied and sampling time $\triangle t$ satisfies certain conditions, the desired signal r and its derivative value are bounded, the error characteristic model of the system can be expressed with the following 2–order difference equation,

$$e(k+1) = f_1(k)e(k) + f_2(k)e(k-1) + g_0(k)v(k) + g_1(k)v(k-1), \tag{6}$$

where $g_0(k) = -g_1(k) + O(\triangle t)$ is slowly time varying, $O(\triangle t)$ represents the high–order infinitesimal term of the sampling time, and $e(k) = y(k) - r(k)$ and $v(k)$ is the bounded sampling control.

For the minimum–phase system, in general the error characteristic model is chosen as follows:

$$e(k+1) = f_1(k)e(k) + f_2(k)e(k-1) + g_0(k)v(k). \tag{7}$$

2.2 Control Object

The problem we study in this paper deals with the nonlinear system described by (1). The control objective is to design a tracking control law which makes sure the output of the nonlinear system follows a reference trajectory.

3. NONLINEAR CHARACTERISTIC MODEL–BASED SMC

In this section, we introduce the characteristic model of nonlinear systems and the SMC method based on this model. The behavior properties of the closed–loop system are described and discussed to illustrate the effect of controllers. Simulations are presented.

3.1 Nonlinear Characteristic Model

In order to verify the possible intervals of nonlinear system characteristic modeling, one example is given. For the stable nonlinear system, characteristic modeling simulation is done with three kinds of control signals. Using Van der Pol equation as the controlled plant, the nonlinear system is

$$\ddot{y} + (y^2 - 1)\dot{y} + y = u. \tag{8}$$

Since (8) can be rewritten as the form of (3), its characteristic model can be described as the style of (4) after it is discreted with sampling time $\triangle t = 0.005s$. Suppose that the control input u has the following three types:

(a) step signal: $u(k) = 10$,
(b) 0.2Hz sinusoid signal: $u(k) = 10\sin(0.4k\pi\triangle t)$,
(c) 0.2Hz square wave signal: $u(k) = 10\text{sgn}[\sin(0.4k\pi\triangle t)]$.

Here we use the recursive least–square method to estimate parameters. Set the forgetting factor $\lambda = 0.97$.

The simulation results in the steady state are listed in Tables 1–3, where the first rows of errors are output estimated errors before parameter estimation while the second rows are output estimated errors after parameter estimation.

Table 1: Simulation results with input (a)

Error	1.9593×10^{-9}		
	-2.7173×10^{-11}		
f_1	1.9915	max 1.9958	min 1.9746
f_2	−0.9916	max −0.9746	min −0.9958
g_0	0.0026	max 0.0027	min 0.0026
g_1	−0.0026	max −0.0026	min −0.0026

Table 2: Simulation results with input (b)

Error	-0.0048		
	-0.0044		
f_1	1.9264	max 2.0083	min 1.9262
f_2	-0.9748	max -0.9695	min -1.0490
g_0	-0.2534	max -0.1800	min -0.2677
g_1	0.2487	max 0.2611	min 0.1761

Table 3: Simulation results with input (c)

Error	-0.0011		
	-0.0009		
f_1	1.9687	max 2.0923	min 1.9796
f_2	-0.9927	max -0.9852	min -1.0983
g_0	0.0003	max 0.0005	min -0.0012
g_1	-0.0004	max -0.0003	min -0.0011

3.2 Sliding Mode Control

To implement a sliding mode controller, it is necessary to design a stable switching surface so that the sliding mode can occur. Based on the nonlinear characteristic model of system (1), the sliding mode are designed as

$$s(k) = \left[\frac{L_1\hat{f}_1(k) + L_2\hat{f}_2(k)}{\eta_1 \mid e(k) \mid^{\mu} + \eta_2} - L_2\hat{f}_2(k)\right] e(k) + L_2\hat{f}_2(k)e(k-1) \tag{9}$$

where $L_1 = 0.382$ and $L_2 = 0.618$ are golden section coefficients, $r(k)$ is the desired output, $e(k) = y(k) - r(k)$, and $\eta_1 > 0$, $\eta_2 > 0$, and μ are adjustable parameters. $\hat{f}_1(k)$ and $\hat{f}_2(k)$ are the estimated values of the corresponding coefficients in (5). The coefficients are estimated by the gradient projection algorithm as follows:

$$\begin{aligned}\hat{\boldsymbol{\theta}}_n(k) &= \hat{\boldsymbol{\theta}}(k-1) + \frac{\lambda_{e1}\boldsymbol{\Phi}(k-1)\left[y(k) - \boldsymbol{\Phi}(k-1)^T\hat{\boldsymbol{\theta}}(k-1)\right]}{\lambda_{e2} + \boldsymbol{\Phi}(k-1)^T\boldsymbol{\Phi}(k-1)} \\ \hat{\boldsymbol{\theta}}(k) &= Pro\left[\hat{\boldsymbol{\theta}}_n(k-1)\right]\end{aligned} \tag{10}$$

where $\boldsymbol{\Phi}(k-1) = [y(k-1),\ y(k-2),\ u(k-1)]^T$ and $\hat{\boldsymbol{\theta}}(k) = \left[\hat{f}_1(k),\ \hat{f}_2(k),\ \hat{g}_0(k)\right]^T$. The positive constants λ_{e1} and λ_{e2} satisfy $0 < \lambda_{e1} < 1$ and $\lambda_{e2} > 0$, respectively. $Pro[\mathbf{x}]$ represents the orthogonal projection from $\mathbf{x}$ to the bounded closed convex set. According to Tables 1–3 we obtains

$$\begin{cases} 1.95 \le \hat{f}_1 \le 2, -1 \le \hat{f}_2 \le -0.95 \\ \hat{g}_0 \in (g_{0\min}, g_{0\max}). \end{cases} \tag{11}$$

Defining

$$\begin{aligned} K_p(k, e(k)) &= k_p(k)\left[\eta_1 \mid e(k) \mid^{\mu} + \eta_2\right]^{-1} \\ k_p(k) &= L_1\hat{f}_1(k) + L_2\hat{f}_2(k) \\ k_d(k) &= -L_2\hat{f}_2(k), \end{aligned} \tag{12}$$

then the nonlinear characteristic model–based sliding mode (9) can be represented as

$$s(k) = K_p(k, e(k))\, e(k) + k_d(k)\left[e(k) - e(k-1)\right]. \tag{13}$$

Moreover, the nonlinear characteristic model based SMC law is

$$\begin{aligned} u(k) = &\Big\{(-\rho s(k) - \left[C_1(k)\hat{f}_1(k) - C_2(k)\right] e(k) \\ &- C_1(k)\hat{f}_2(k)e(k-1) - \vartheta \mathrm{sgn}\left[s(k)\right]\Big\} \\ &/\left\{\left[C_1(k)\hat{f}_1(k) - C_2(k)\right]\hat{g}_0(k)\right\}, \end{aligned} \tag{14}$$

where ρ and ϑ are positive constants, $C_1(k) = K_p(k, e(k)) + k_d(k)$, and $C_2(k) = k_d(k)$.

Theorem 3. If the error characteristic model of system (1) can be expressed with (7), under the control law (14), the tracking error of system (1) converges to zero with $\frac{\vartheta}{1-\rho} < |s(k)|$.

Proof. Choosing Lypapunov function $V(k) = \frac{1}{2}s(k)^2$, the behavior of $s(k)$ can be prescribed as

$$s(k+1) = C_1(k+1)e(k+1) + C_2(k+1)e(k). \tag{15}$$

Substituting (7) and (14) into (15) yields

$$\begin{aligned} s(k+1) = &-\rho\frac{C_1(k+1)}{C_1(k)}s(k) + \frac{C_1(k+1)}{C_1(k)}C_2(k)e(k) \\ &- C_2(k+1)e(k) - \vartheta\frac{C_1(k+1)}{C_1(k)}\mathrm{sgn}\left[s(k)\right]. \end{aligned} \tag{16}$$

According to Wu et al. [2001] , $K_p(k, e(k))$ and $k_d(k)$ are bounded and $\hat{f}_1(\infty)$ and $\hat{f}_2(\infty)$ barely vary when $k > N$. Then we obtain

$$s(k+1) = -\rho s(k) - \vartheta \mathrm{sgn}\left[s(k)\right] \tag{17}$$

and

$$\begin{aligned} &[s(k+1) - s(k)]\,\mathrm{sgn}\left[s(k)\right] = (-1-\rho)|s(k)| - \vartheta < 0, \\ &[s(k+1) + s(k)]\,\mathrm{sgn}\left[s(k)\right] = (1-\rho)|s(k)| - \vartheta > 0. \end{aligned} \tag{18}$$

Hence the control law (14) makes (9) converge to zero in finite time. Observing $s(k) = 0$ in sliding phase, it follows that

$$e(k) = \frac{C_1(k)}{C_1(k) + C_2(k)}e(k-1). \tag{19}$$

Substituting (11) into(12),we have $C_1(k) > 0$ and $C_2(k) > 0$, which result in $0 < \frac{C_1(k)}{C_1(k)+C_2(k)} < 1$. Thus the error converges to zero, which completes the proof.

3.3 Simulation Results

In this part, we give the simulation results of the proposed method to verify the effectiveness and performance of the designed controller.

For the nonlinear system (8), the output is expected to track a desired signal r. Traditionally, we take $s = c_{h1}\dot{e} + c_{h2}e$ as the sliding mode and $u = -T\mathrm{sgn}(s)$ as the controller. The simulation result in Fig. 1 shows the control effect loses stability. Then we choose the nonlinear sliding mode as shown in (9) and $u = -T\mathrm{sgn}(s)$ as controller. Fig. 2 shows that the designed sliding mode can solve tracking problem but the tracking error has chattering due to the controller. The designed controller in this paper, however, as shown in Fig. 3, insures the fast maneuver and stability without chattering. The phase phase of designed sliding mode and controller is shown in Fig. 4, which shows that the sliding mode and the tracking error can converge to zero.

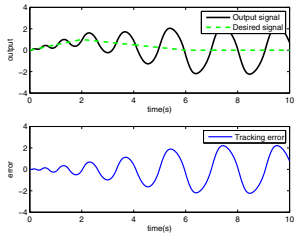

Fig. 1. The linear sliding mode controller with $c_{h1} = 5$, $c_{h2} = 1$, and $T = 15$,

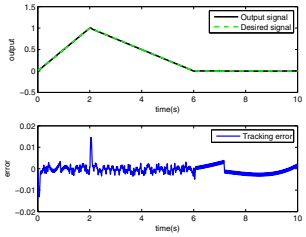

Fig. 2. The nonlinear sliding mode and $u = -T\text{sgn}(s)$ with $\eta_1 = 10$, $\eta_2 = 1$, $\mu = 2$, and $T = 15$.

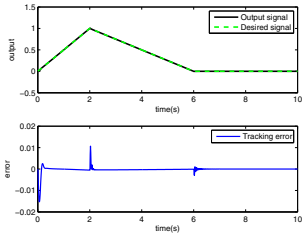

Fig. 3. The nonlinear sliding mode and the designed controller with $\eta_1 = 10$, $\eta_2 = 1$, $\mu = 2$, $\rho = 0.8$, and $\vartheta = 1 \times 10^{-4}$

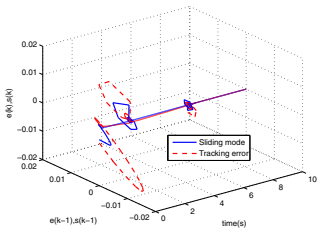

Fig. 4. Sliding mode and output error phase plane

Remark 1. The proportionality coefficient $K_p\,(k, e(k))$ is related to $k_p(k)$ and varies with $e(k)$. Adjustable parameters μ, η_1, and η_2 are related to control performance. Usually, the dynamic process performance of the overall system can be improved as η_1 grows, but it will cause vibration in the steady state. The growth of η_2 suppresses the vibration whereas reduces the dynamic process performance in the meantime. Therefore, how to determine the value of η_1 and η_2 is the key question of the SMC based on the nonlinear characteristic model.

4. SATELLITE ATTITUDE CONTROL

The application of the nonlinear characteristic model–based SMC to the three–axis stabilized complex satellite with large flexible solar panels is investigated in this section.

4.1 Kinematics model of satellite

Reconnaissance the satellite is usually treated as a rigid body with many flexible structures. The dynamics model of satellite and vibration model of solar wings are (see Kim et al. [2004])

$$\boldsymbol{I}_s\dot{\boldsymbol{\omega}}_s + \boldsymbol{\omega}_s^{\times}\boldsymbol{I}_s\boldsymbol{\omega}_s + \boldsymbol{F}_{sa}\ddot{\boldsymbol{\eta}}_{sa} = \boldsymbol{T}_T \tag{20}$$

$$\ddot{\boldsymbol{\eta}}_{sa} + 2\xi_{sa}\boldsymbol{\omega}_{sa}\dot{\boldsymbol{\eta}}_{sa} + \boldsymbol{\omega}_{sa}^2\boldsymbol{\eta}_{sa} + \boldsymbol{F}_{sa}^T\dot{\boldsymbol{\omega}}_s = \boldsymbol{0} \tag{21}$$

where $\boldsymbol{\omega}_s = [\omega_x,\ \omega_y,\ \omega_z]^T \in \Re^{3\times 1}$ is the angular velocity, $\boldsymbol{I}_s \in \Re^{3\times 3}$ is the rotational inertia of satellite, $\boldsymbol{T}_T \in \Re^{3\times 1}$ is the aggregate external torque, $\boldsymbol{\eta}_{sa} \in \Re^{m\times 1}$ is the vibration modal coordinates array of solar wings, $\boldsymbol{\omega}_{sa} \in \Re^{m\times m}$ is the modal frequency matrix of solar wings vibration, ξ_{sa} is the vibration damping ratio of solar wings, and $\boldsymbol{F}_{sa} \in \Re^{3\times m}$ is the coupling coefficient matrix between wings and body. Define $\boldsymbol{\omega}_s^{\times}$ as

$$\boldsymbol{\omega}_s^{\times} = \begin{bmatrix} 0 & -\omega_z & -\omega_y \\ \omega_z & 0 & -\omega_x \\ -\omega_y & \omega_x & 0 \end{bmatrix}. \tag{22}$$

Quaternion are generally used in the on-board attitude presentation, which are defined by

$$q_0 = \cos(\frac{\alpha}{2}),\ \boldsymbol{q} = [\gamma_1\sin(\frac{\alpha}{2}),\ \gamma_2\sin(\frac{\alpha}{2}),\ \gamma_3\sin(\frac{\alpha}{2})]^T \tag{23}$$

where $[\gamma_1,\ \gamma_2,\ \gamma_3]^T$ is the principle axis from the current attitude to the reference attitude and α is the principle angle. Kinematics model is established referring to the aforementioned frame and quaternion:

$$\dot{\boldsymbol{q}} = \frac{1}{2}(\boldsymbol{q}^{\times} + q_0\boldsymbol{I})\boldsymbol{\omega}_s,\ \dot{q}_0 = -\frac{1}{2}\boldsymbol{q}^T\boldsymbol{\omega}_s. \tag{24}$$

4.2 Design of Controller

Define

$$\boldsymbol{x} = \left[q_0,\ \boldsymbol{q}^T,\ \boldsymbol{\eta}_{sa}^T,\ \dot{\boldsymbol{\eta}}_{sa}^T,\ \boldsymbol{\omega}_s^T\right]^T,\ \boldsymbol{u} = \boldsymbol{T}_T \tag{25}$$

and take 5–order vibration modal of solar wings. The system (20), (21), and (24) can be rewritten as:

$$\boldsymbol{A}_1\dot{\boldsymbol{x}} = \boldsymbol{A}_2(\boldsymbol{x}) + \boldsymbol{B}\boldsymbol{u} \tag{26}$$

where

$$\boldsymbol{A}_1 = \begin{bmatrix} 1 & \boldsymbol{O}_{1\times 3} & \boldsymbol{O}_{1\times 5} & \boldsymbol{O}_{1\times 5} & \boldsymbol{O}_{1\times 3} \\ \boldsymbol{O}_{3\times 1} & \boldsymbol{I}_{3\times 3} & \boldsymbol{O}_{3\times 5} & \boldsymbol{O}_{3\times 5} & \boldsymbol{O}_{3\times 3} \\ \boldsymbol{O}_{5\times 3} & \boldsymbol{O}_{5\times 3} & \boldsymbol{I}_{5\times 5} & \boldsymbol{O}_{5\times 5} & \boldsymbol{O}_{5\times 3} \\ \boldsymbol{O}_{5\times 1} & \boldsymbol{O}_{5\times 3} & \boldsymbol{O}_{5\times 5} & \boldsymbol{I}_{5\times 5} & \boldsymbol{F}_{sa5\times 3}^T \\ \boldsymbol{O}_{3\times 1} & \boldsymbol{O}_{3\times 3} & \boldsymbol{O}_{3\times 5} & \boldsymbol{F}_{sa3\times 5} & \boldsymbol{I}_{s3\times 3} \end{bmatrix}$$

$$\boldsymbol{A}_2(\boldsymbol{x}) = \begin{bmatrix} -\frac{1}{2}\boldsymbol{q}^T\boldsymbol{\omega}_s \\ \frac{1}{2}\left(\boldsymbol{q}^{\times} + q_0\boldsymbol{I}\right)\boldsymbol{\omega}_s \\ \dot{\boldsymbol{\eta}}_{sa} \\ -2\xi_{sa}\boldsymbol{\omega}_{sa}\dot{\boldsymbol{\eta}}_{sa} - \boldsymbol{\omega}_{sa}^2\boldsymbol{\eta}_{sa} \\ -\boldsymbol{\omega}_s^{\times}\boldsymbol{I}_s\boldsymbol{\omega}_s \end{bmatrix},\ \boldsymbol{B} = \begin{bmatrix} \boldsymbol{O}_{1\times 3} \\ \boldsymbol{O}_{3\times 3} \\ \boldsymbol{O}_{5\times 3} \\ \boldsymbol{O}_{5\times 3} \\ \boldsymbol{I}_{1\times 3} \end{bmatrix}.$$

According to Wu et al. [2001], since (26) can be rewritten as the form of (3), the characteristic model of the system (26) is chosen as follows:

$$q_i(k+1) = f_{1i}(k)q_i(k) + f_{2i}q_i(k_1) + g_{0i}(k)u_i(k), \tag{27}$$

where $1.95 \le f_{1i} \le 2$, $-1 \le f_{2i} \le -0.95$, $g_{0min} \le g_{0i} \le g_{0max}$, and $i = 1,\ 2,\ 3$. The coefficients estimated by the

gradient projection algorithm have been shown in Section 2.

The sliding modes are designed as

$$s_i(k) = \left[\frac{L_1\hat{f}_{1i}(k) + L_2\hat{f}_{2i}(k)}{\eta_{1i}|e_i(k)|^{\mu} + \eta_{2i}}\right] e_i(k) + L_2\hat{f}_{2i}(k)e_i(k-1), \tag{28}$$

where $q_{ri}(k)$ are desired quaternion, $e_i(k) = q_i(k) - q_{ri}(k)$, and $i = 1,\ 2,\ 3$.

Accordingly, the controllers are depicted as

$$u_i(k) = \Big\{(-\rho s_i(k) - \left[C_{1i}(k)\hat{f}_{1i}(k) - C_{2i}(k)\right] e_i(k) - C_{1i}(k)\hat{f}_{2i}e_i(k-1) - \vartheta \mathrm{sgn}\left[s_i(k)\right]\Big\} / \Big\{\left[C_{1i}(k)\hat{f}_{1i}(k) - C_{2i}(k)\right]\hat{g}_{0i}(k)\Big\}, \tag{29}$$

where $C_{1i}(k) = K_{pi}(k, e_i(k)) + k_{di}(k)$, $C_{2i}(k) = k_{di}(k)$, and $i = 1,\ 2,\ 3$.

4.3 Numerical Simulations

The designed controller is applied to a sun synchronous orbit satellite. The main parameters of the flexible satellite can be described as:

$$\boldsymbol{I}_s = \begin{bmatrix} 6393.31 & 26.95 & -21.09 \\ 26.95 & 4737.30 & 1868.48 \\ -21.09 & 1868.48 & 8361.13 \end{bmatrix} \left(kg \cdot m^2\right),$$

$$\boldsymbol{\omega}_{sa} = diag(1.02,\ 1.24,\ 1.92,\ 2.86,\ 3.88)(rad/s),$$

$$\xi_{sa} = 0.005.$$

There is a solar panel control problem for a sun synchronous orbit satellite, which has one degree freedom single solar panel driven by a constant velocity to point to the sun. Due to this problem, coupling coefficient matrix between wings and body is time varying as follows:

$$\boldsymbol{F}_{sa} = \boldsymbol{C}^T(\theta)\boldsymbol{F}_{s0}.$$

where

$$\boldsymbol{C}(\theta) = \begin{bmatrix} \cos(\theta) & 0 & -\sin(\theta) \\ 0 & 1 & 0 \\ \sin(\theta) & 0 & \cos(\theta) \end{bmatrix},$$

$$\boldsymbol{F}_{s0}^T = \begin{bmatrix} 0.335908 & 18.3213 & -20.8864 \\ -0.0100547 & -20.8362 & -26.3452 \\ -29.7119 & 0.0752216 & 0.561621 \\ 20.0637 & -0.364224 & -0.790376 \\ 0.0240133 & 10.2219 & 27.968 \end{bmatrix}.$$

The closed system logic structure is shown in Fig. 5.

In this simulation, the initial quaternion value is set to $\boldsymbol{q} = [0.0245,\ 0.28422,\ 0.3853]^T$. The final target quaternion value is $\boldsymbol{q} = [0,\ 0,\ 0]^T$. For the sliding mode, the parameters are $\mu = 1$, $\eta_1 = 50$, and $\eta_2 = 0.2$. The parameters of controller are tuned as $\rho = 0.8$ and $\vartheta = 1 \times 10^{-4}$.

First we consider the rotational inertia of satellite as $\boldsymbol{I}_s$. The simulation results are shown in Figs. 6–9.

The simulation results show that convergent times of three–axis are very close. Maneuvering angles are 5°, 30°, and 50°, respectively. The rapid maneuvering performance and pointing accuracy are significantly improved. The interference of the solar wings vibration with pointing to the sun is suppressed. As can be seen from the phase plane in Figs. 10–12, the nonlinear characteristic model

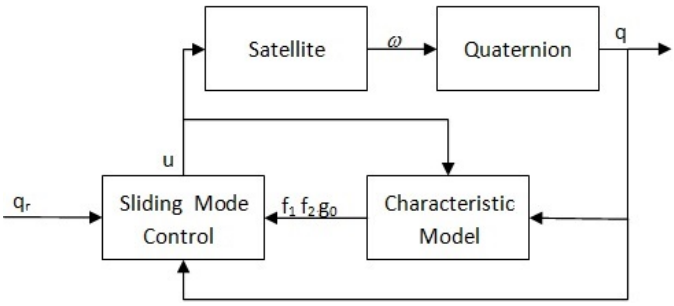

Fig. 5. Control logic block diagram for satellite

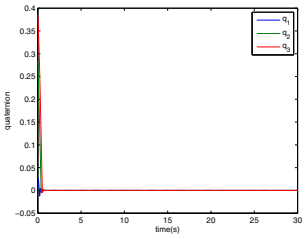

Fig. 6. Quaternion responses

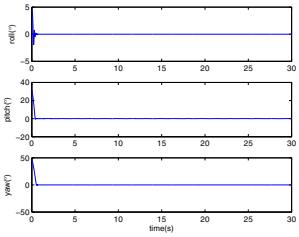

Fig. 7. Attitude angles

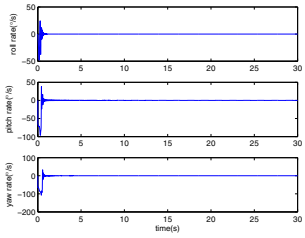

Fig. 8. Angular rates

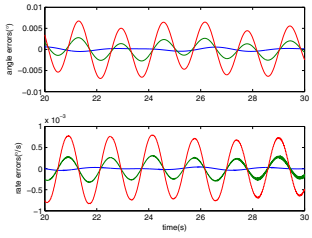

Fig. 9. Angle and velocity errors

based sliding mode and the controller demonstrate a faster convergence and better robustness compared to Zhou et al. [2013].

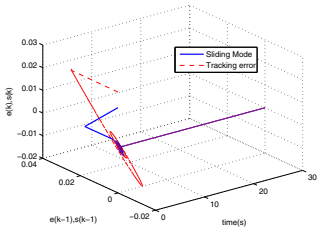

Fig. 10. The sliding mode and tracking error of the first channel

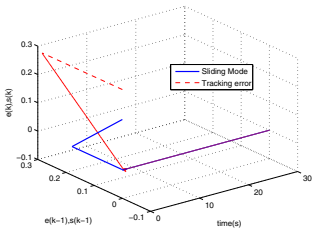

Fig. 11. The sliding mode and tracking error of the second channel

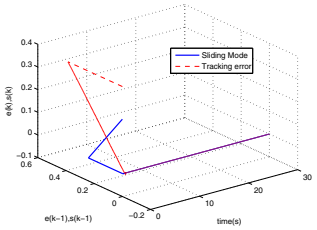

Fig. 12. The sliding mode and tracking error of the third channel

Then the rotational inertia of satellite is considered as $1.5\boldsymbol{I}_s$ and $0.5\boldsymbol{I}_s$, respectively. The simulation results in Table 4 illuminate that although there has high uncertainty of the satellite, the proposed controller can provide a satisfactory tracking result.

Table 4: Simulation results

Rotational inertia	$1.5\boldsymbol{I}_s$	$0.5\boldsymbol{I}_s$
Maneuvering performance	$27s$	$29s$
Pointing accuracy	$0.005°$	$0.005°$
Stable performance	$25s$	$23s$
Attitude stability	$0.001°$	$0.001°$

5. CONCLUSION

A nonlinear sliding mode for SMC based on the characteristic model has been proposed in this paper. The proposed controller has been used for controlling a class of nonlinear systems to track the desired signal and guarantee the stability. We have shown that the benefit of the nonlinear sliding mode surface has possibly improved the convergence and robustness of the systems. This has been illustrated on a real application satellite model. The simulation results have been presented to confirm the effectiveness of the controller.

REFERENCES

A.M. Zanchettin and M. Lovera. H_∞ attitude control of magnetically actuated satellites. In *IFAC World Congress*, 2011.

B.B. Zhang, K. Liu, and J.H. Xiang. A stabilized optimal nonlinear feedback control for satellite attitude tracking. *Aerosp. Sci. Technol.*, 27(1):17–24, 2013.

B. Kim, Y. Kim, H. Bang, M. Tahk, and S. Hong. *Flight dynamics and control*, first ed. Kyungmoon Publishers, Seoul, 2004.

B. Meng, H.X. Wu, Z.L. Lin, and G. Li. Characteristic model based control of the X–34 reusable launch vehicle in its climbing phase. *Sci. in China (Series F)*, 52(11):2216–2225, 2009.

C.Y. Sun, C.X. Mu, and Y, Yu. Some control problems for near space hypersonic vehicles. *Acta Autom. Sinica*, 39(11):1901–1913, 2013.

D. Peaucelle, A. Drouot, C. Pittet, and J. Mignot. Simple adaptive control without passivity assumptions and experiments on satellite attitude control demeter benchmark. In *IFAC World Congress*, 2011.

D. Zhou, Y. Guo, Q. Chen, and W. Hu. Cell membrane discharge model enlightened robust attitude maneuvering control for flexible spacecraft. *J. of Astron.*, 34(2):222–230, 2013.

H. Wong, M.S.de Queiroz, and V. Kapila. Adaptive tracking control using synthesized velocity from attitude measurements. *Automatica*, 37(6):947–953, 2001.

H.X. Wu, Y. W. Liu, Z.H. Liu, and Y.C. Xie. Characteristic modeling and the control of flexible structure. *Sci. in China (Series F)*, 44(4):278–291, 2001.

Q. Hu, B. Xiao, and M.I. Friswell. Fault tolerant control with H_∞ performance for attitude tracking of flexible spacecraft. *IEEE Trans. Control Theory Appl.*, 6(10):1388–1399, 2012.

S.N. Singh. Rotational maneuvers of nonlinear uncertain spacecraft. *IEEE Trans. Aerosp. Electron. Syst.*, 24(2):114–123, 1988.

T. Wen and K. Kreutz–Delgado. The attitude control problem. *IEEE Trans. Autom. Control*, 36(10):1148–1142, 1991.

W. Luo, Y.C. Chu, and K.V. Ling. Inverse optimal adaptive control for attitude tracking of spacecraft. *IEEE Trans. Autom. Control*, 50(11):1639–1654, 2005.

X.H. Yu, B. Wang, and X.J. Li. Computer–controlled variable structure systems: the state–of–the–art. *IEEE Trans. Ind. Inform.*, 8(2):197–205, 2012.

Y.Q. Xia, Z. Zhu, M.Y. Fu, and S. Wang. Attitude tracking of rigid spacecraft with bounded disturbance. *IEEE Trans. Ind. Electron.*, 58(2):647–659, 2011.

Y.X. Zhang, M.W. Sun, and Z.Q. Chen. Finite–time convergent guidance law with impact angle constraint based on sliding–mode control. *Nonlinear Dyn.*, 70(1):619–625, 2012.

Z. Zhen and J. Huang. Attitude tracking and distrubance rejection of rigid spacecraft by adapitve control. *IEEE Trans. Autom. Control*, 54(3):600–605, 2009.